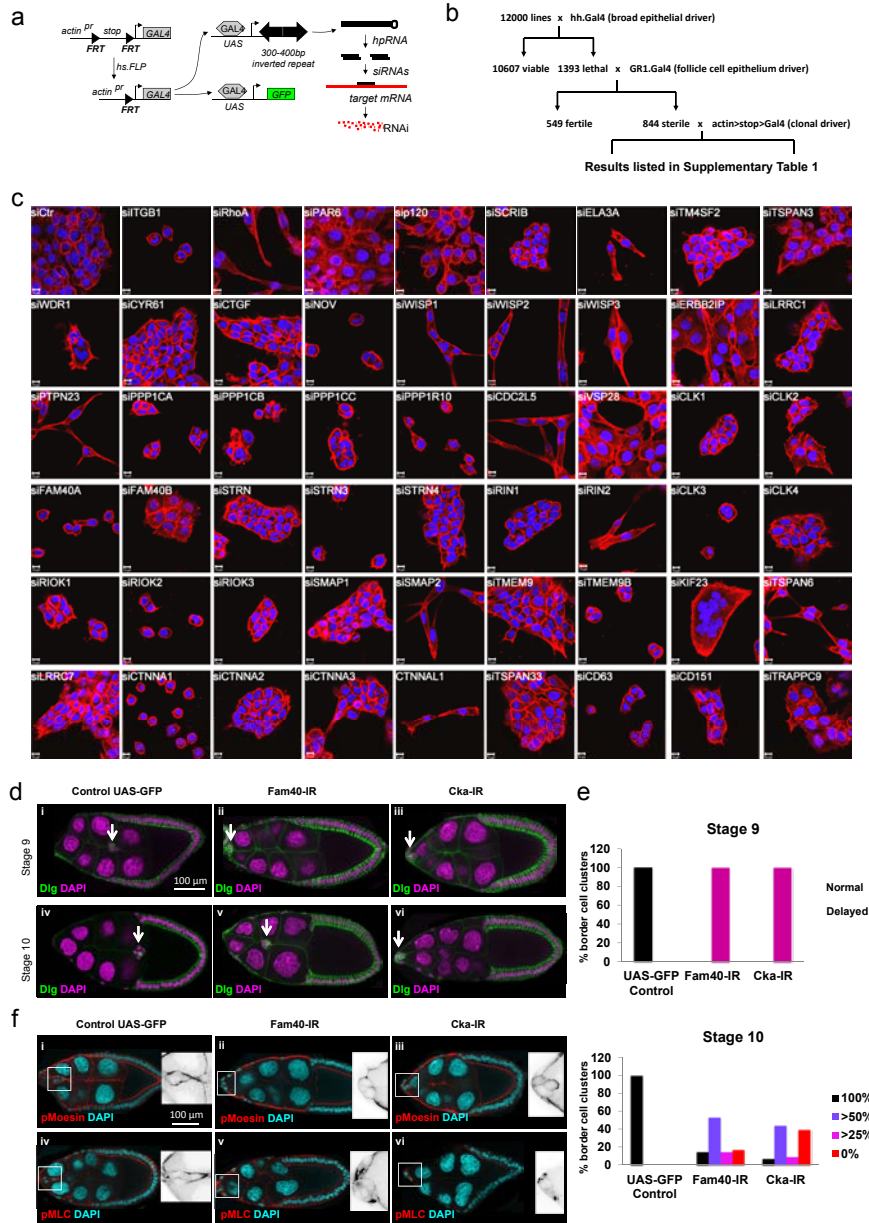
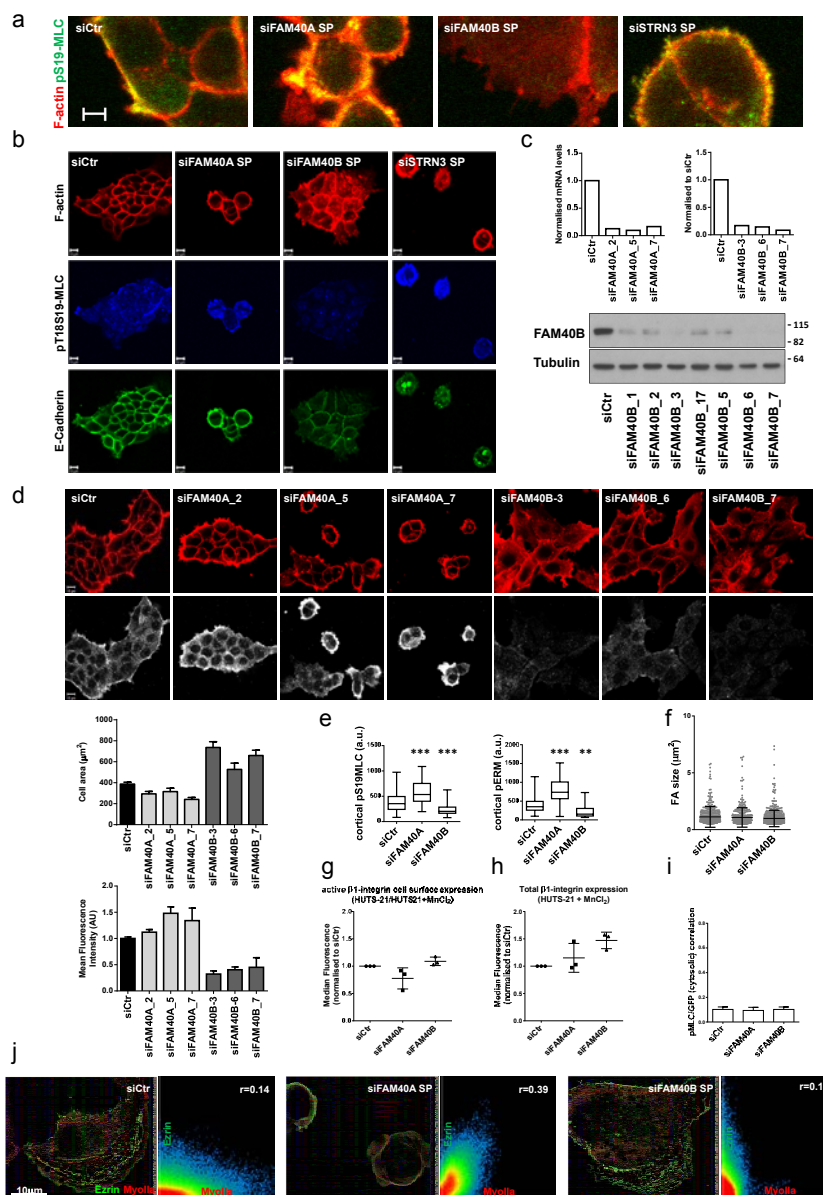


DOI: 10.1038/ncb3083



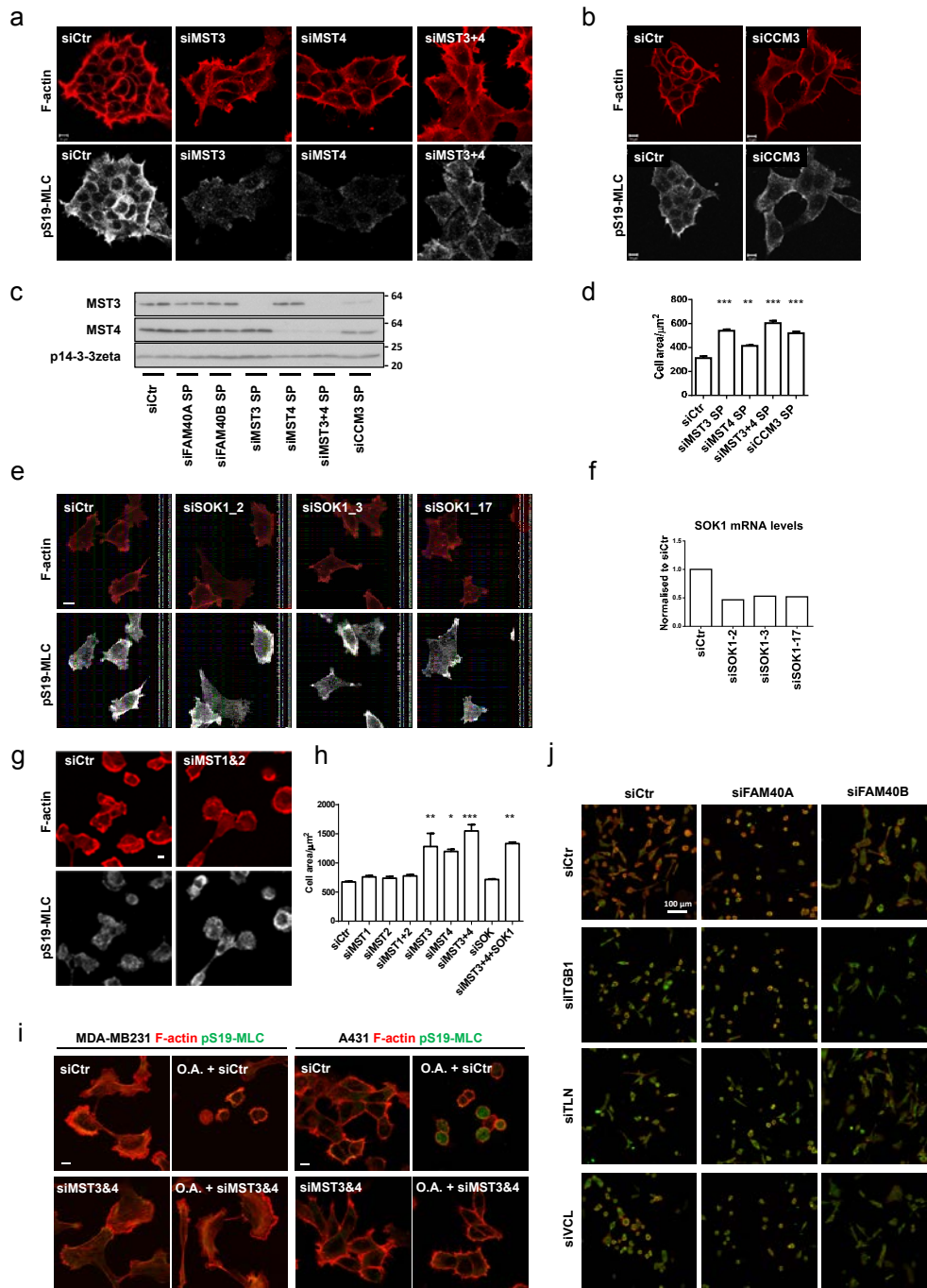
Supplementary Figure 1 RNAi screen in the egg chamber of *Drosophila melanogaster* and in human A431 carcinoma cells. RNAi screen targeting genes that are required for border cell migration and actin organisation in follicle epithelial cells within the *Drosophila* egg chamber. **(a)** Schematic view of the screening strategy. **(b)** Flow diagram of the screen. siRNA lines crossed on to the hh.GAL4 driver were assumed to have no strong phenotype within the egg chamber (either border cell or follicular epithelium) if the flies were healthy and viable – these were not further analysed. The 1393 lethal siRNA lines were further analysed for egg chamber phenotypes by crossing the Gr1. GAL4 driver – 594 of these lines were fertile and therefore not analysed further. The remaining 844 lines were analysed in more detail. **(c)** Cell morphologies observed upon siRNA depletion in human A431 carcinoma cells. A431 cells were transfected with the indicated siRNAs and plated on collagen-I/matrigels. (n=3 screens). The cells were fixed and stained with Phalloidin-TRITC (red) and DAPI (blue) 72h post-transfection. Only genes affecting the cell morphology

are shown. **(d)** Border cell migration delay in the CG11526 (FAM40) and *CKA* (STRN) RNAi flies. Representative images of the *Drosophila melanogaster* egg chamber at stage 9 and 10. The egg chambers were stained for the basolateral marker Discs Large (Dlg, green) and DAPI (magenta). RNAi expression was driven in border cells using a Gr1-Gal4 driver. **(e)** Quantification of border cell clusters that reached their destination at stage 9 (upper histogram, n=animals; *Ctrl*, 43; *FAM40ARNAi*, 23; *CKARNAi*, 28). Estimation of the distance travelled by the border cell cluster at stage 10 (lower histogram, n=animals; *Ctrl*, 64; *FAM40ARNAi*, 47; *CKARNAi*, 43): 100% - reached the oocyte; >50% - travelled more than half the distance toward the oocyte; >25% - travelled more than one fourth the distance toward the oocyte; 0% - did not leave the anterior part of the egg chamber. **(f)** Representative images of the egg chamber at stage 9 stained for with DAPI (cyan) and pMoesin (red, upper panels) or pMyosin2 (red, lower panels). The insets represent a zoomed area. Scale bars, 10 µm, unless indicated otherwise.



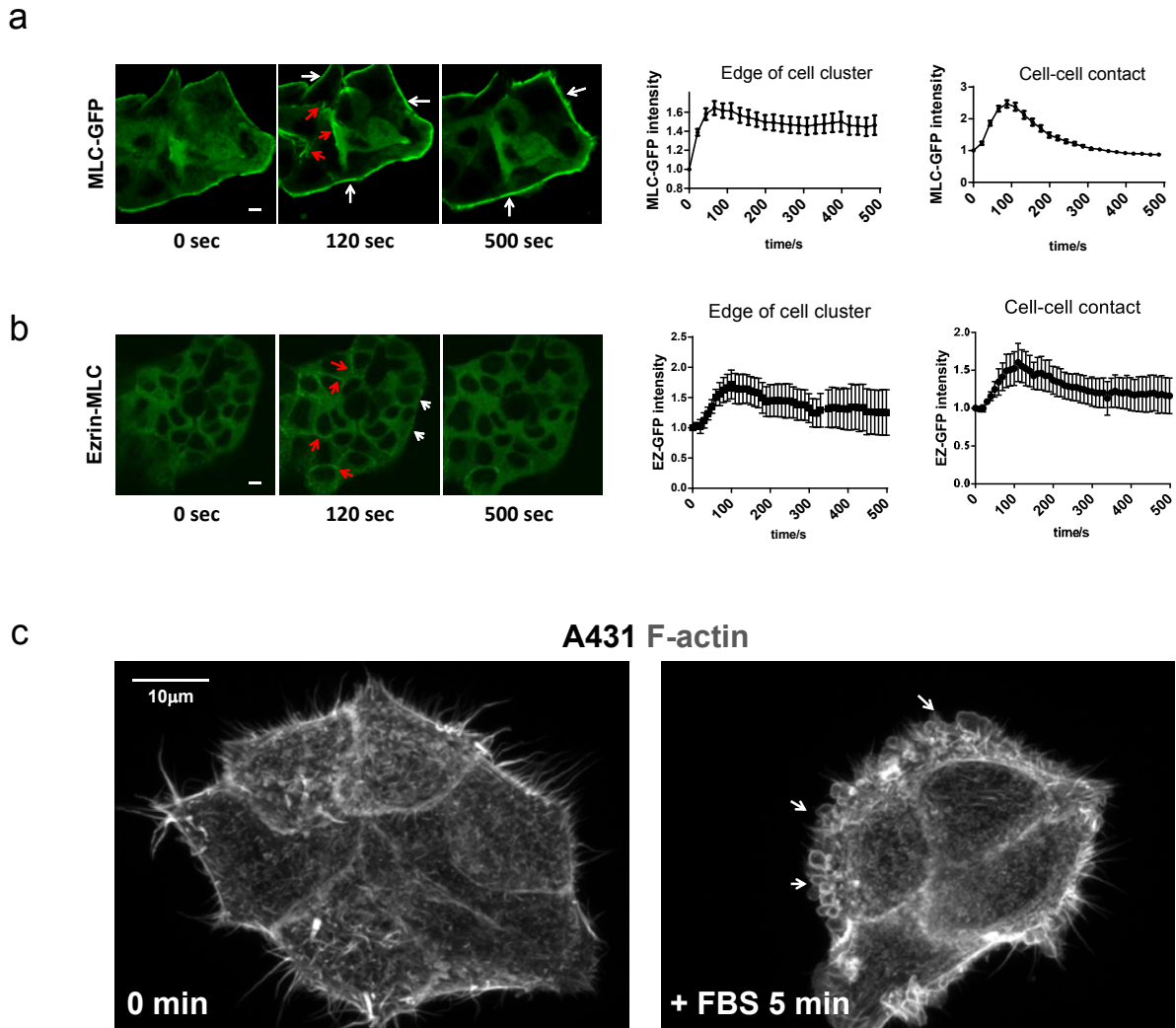
Supplementary Figure 2 Epithelial organisation upon FAM40A, FAM40B and STRN3 depletion in human cancer cells. **(a-b)** siRNA depleted A431 cells plated on collagen-I/matrigels. Cells were fixed 72h post-transfection and stained **(a)** against pS19-MLC (green) and **(b)** pT18S19-MLC (blue) and E-Cadherin (green). F-actin is stained with Phalloidin-TRITC (red). **(c)** siRNA knockdown efficiency +/-s.e.m of FAM40A and FAM40B mRNA in A431 cells. Immunoblotting analysis of FAM40B protein levels upon FAM40B depletion. **(d)** Deconvolution of siRNA oligos in A431 cells plated on collagen-I/matrigel. Cells were stained 72h post-transfection against pS19-MLC2 (white) and F-actin (red). Quantification of A431 cell area +/-s.e.m (upper histogram, n=fields of cells; Ctr, 19; siFAM40A_2, 9; siFAM40A_5, 6; siFAM40A_7, 5; siFAM40B-3, 12; siFAM40B-6, 6; siFAM40B-7, 7) and mean fluorescence pS19-MLC2 intensities +/-s.e.m (lower histogram, n=fields of cells; Ctr, 10; siFAM40A_2, 6; siFAM40A_5, 4; siFAM40A_7, 4; siFAM40B-3, 6; siFAM40B-6, 6; siFAM40B-7, 6). **(e)** Quantification of mean fluorescence cortical intensities of pS19-MLC2 (left panel, n=cells; Ctr, 33; siFAM40A, 46; siFAM40B, 47) and pERM (right panel, n=cells; Ctr, 29; siFAM40A, 35; siFAM40B, 43) in MDA-MB231 cells. Box and whiskers graph: Line=Median, Box=distribution of 50% of values, whiskers=min. to max. **(f)** siRNA depleted MDA-MB231 cells were fixed 72h post-transfection.

Focal adhesions were stained with phospho-tyrosine antibody (cl. 4G10), and thin sections of the focal adhesions in the basal plasma membrane were acquired using confocal microscopy. Morphometric analysis was performed on individual cells. Two independent experiments were conducted and 20-25 cells quantified. n=focal adhesions; Ctr, 468; siFAM40A, 401; siFAM40B, 558). **(g-h)** Cell surface expression of integrin β1 (ITGB1) using flow cytometry was performed on MDA-MB231 cells 72h post-transfection. Cell surface expression of ITGB1 +/-s.d. was detected using the HUTS-21 antibody detecting the active form with or without the presence of 0.5mM MnCl₂ to activate all integrins on the cell surface (n=3 experiments). **(i)** Quantification of pS19-MLC2 and cytosolic GFP co-localisation +/-s.e.m. (n=cells; siCtr, 25; siFAM40A, 16; siFAM40B, 17). **(j)** siRNA depleted MDA-MB231-Ezrin-GFP cells were fixed 72h post-transfection. Cells were stained for MyoIIA (red), and thin 150 nm sections were acquired using Structured Illumination Microscopy (left panels). The spatial correlation (r) between Ezrin-GFP (green) and MyoIIA (red) was then determined upon FAM40A and FAM40B depletion and compared to control cells (right panels). Statistical test were performed using 1way ANOVA, Sidak's multiple comparison test, *P<0.05, **P<0.01, ***P<0.001. All experiments were conducted at least 3 independent times. Scale bars, 10 µm, unless indicated otherwise.



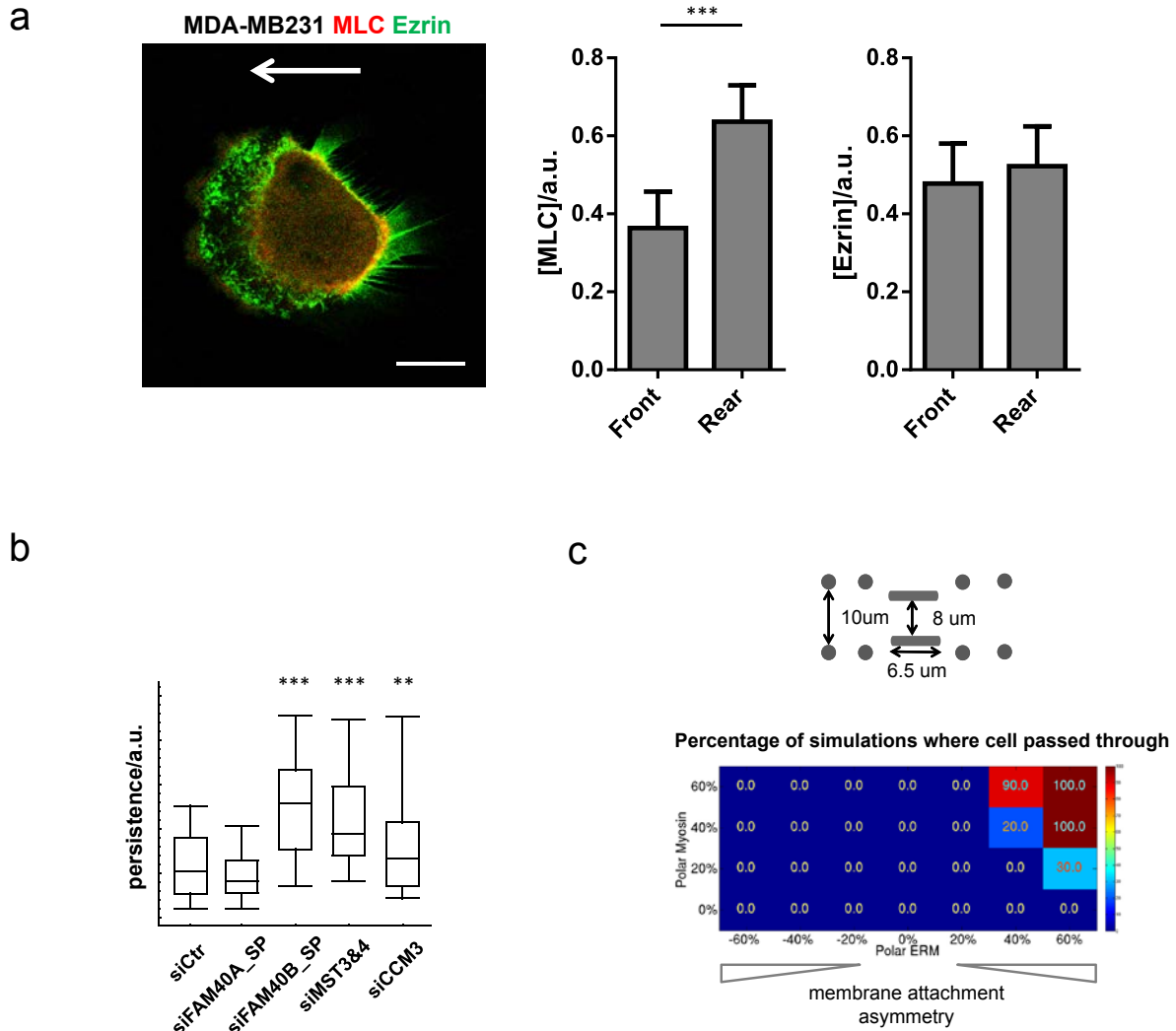
Supplementary Figure 3 Epithelial organisation upon MST1, MST2, MST3, MST4, MST3&4, SOK1 and CCM3 depletion in A431 cells. (a-b) The human genes, MST3, MST4, MST3&4 and CCM3, were depleted in A431 cells using siRNA smart pools and plated on collagen-I/matrigels. The cells were fixed 72h post-transfection and stained against pS19-MLC (white) and F-actin (red). (c) Immunoblotting analysis shows the knockdown efficiency of MST3 and MST4 proteins upon siRNA depletion. (d) Quantification of A431 cell area +/-s.e.m upon siRNA depletion and plating on collagen-I/matrigels (n=fields of cells; siCtrl, 17; siMST3, 8; siMST4, 6; siMST3&4, 13; siCCM3, 2). (e) Deconvolution of three SOK1 siRNA oligos in MDA-MB231 cells plated on collagen-I/matrigel. Cells were stained 72h post-transfection against pS19-MLC2 (white) and F-actin (red). (f) Knockdown efficiency of SOK1 mRNA using three individual siRNA oligos as compared to control cells. (g) Double depletion of MST1&2 in MDA-MB231 cells using siRNA smart pools. The cells

were fixed 72h post-transfection and stained against pS19-MLC (white) and F-actin (red). (h) Quantification of MDA-MB231 cell area +/-s.e.m upon siRNA depletions (n=fields of cells; siCtrl, 19; siMST1, 5; siMST2, 5; siMST1&2, 8; siMST3, 2; siMST4, 2; siMST3&4, 14; siSOK, 2; siMST3&4&SOK, 2). (i) Double depletion using smart pools of FAM40A or FAM40B with either ITGB1, talin (TLN) or vinculin (VCL). MDA-MB231 cells were stained 72h post-transfection against pS19-MLC2 (green) and F-actin (red). (j) Epistasis experiments in MDA-MB231 (left panel) and A431 cells (right panel) show that MST3&4 depletion rescues the contractile phenotype observed upon Okadaic acid treatment. The cells were fixed 72h post-transfection and stained against pS19-MLC (green) and F-actin (red). All statistical test were performed using 1way ANOVA, Sidak's multiple comparison test, * $P < 0.05$, ** $P < 0.01$, *** $P < 0.001$. All experiments were conducted at least 3 independent times. Scale bars, 10 μ m, unless indicated otherwise.



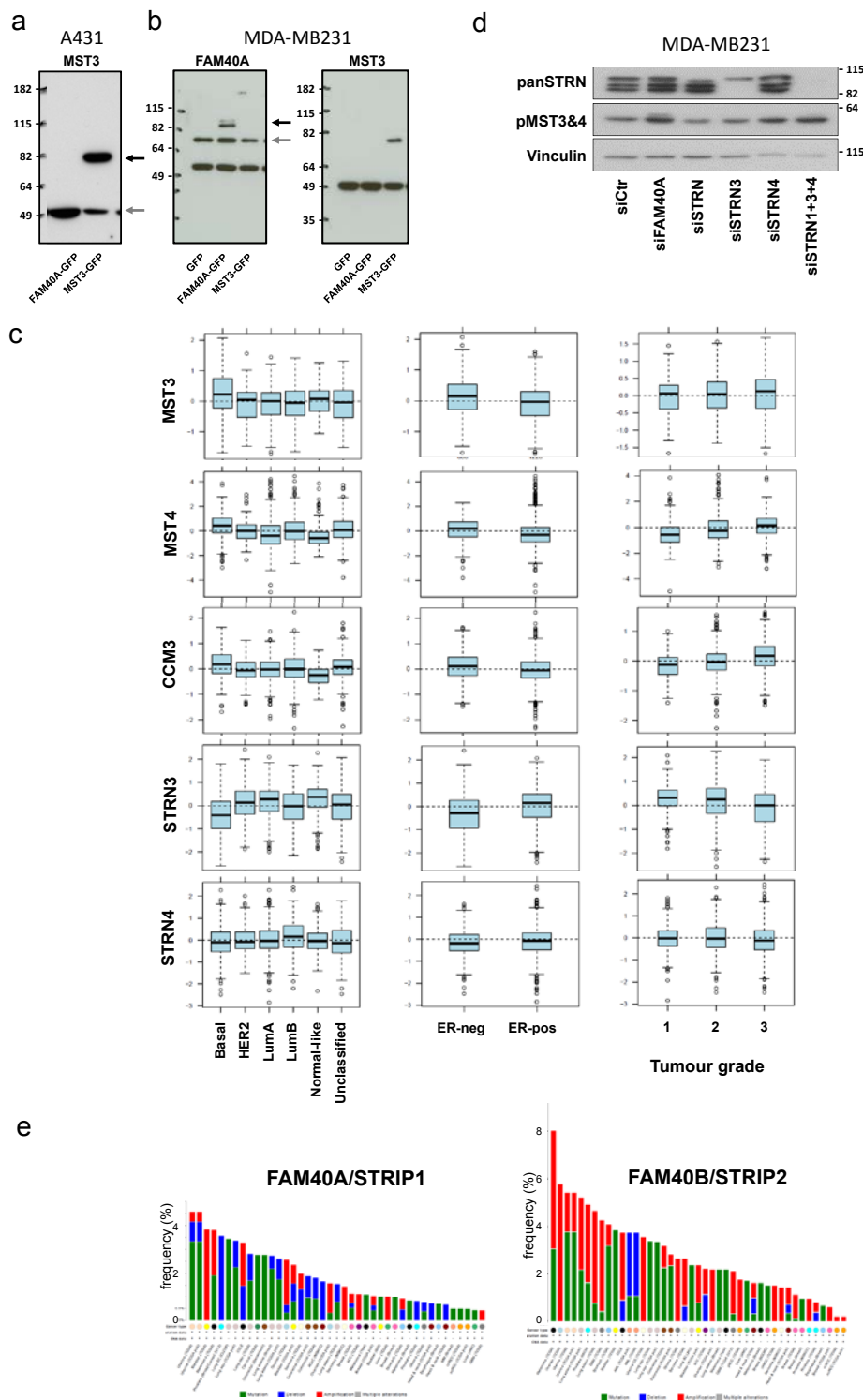
Supplementary Figure 4 Temporal regulation of MLC and Ezrin. (a-b) Serum stimulation of serum starved A431-MLC-GFP (a) and A431-Ezrin-GFP cells (b) induces an immediate translocation of MLC-GFP and Ezrin-GFP to the actomyosin network at the outer edge (white arrows) of A431 cell clusters and at cell-cell junctions (red arrows). Quantification of the serum-induced MLC-GFP and Ezrin-GFP translocation \pm s.e.m was performed by normalising the mean fluorescence intensity at cell border (left graph) and cell-cell junctions

(right graph) to the mean fluorescence intensity of the adjacent cytosolic fraction. n = regions of individual measurements (63x) at edge of cluster and cell-cell contacts; MLC, 70; Ez, 35. The values are pooled from three independent experiments. (c) F-actin staining of serum starved A431 cells and after 5 minutes of FCS stimulation. FCS stimulation induces slight blebbing at the cortex of the cells. Blebs are indicated by white arrows. All experiments were conducted at least 3 independent times. Scale bars, 10 μ m.



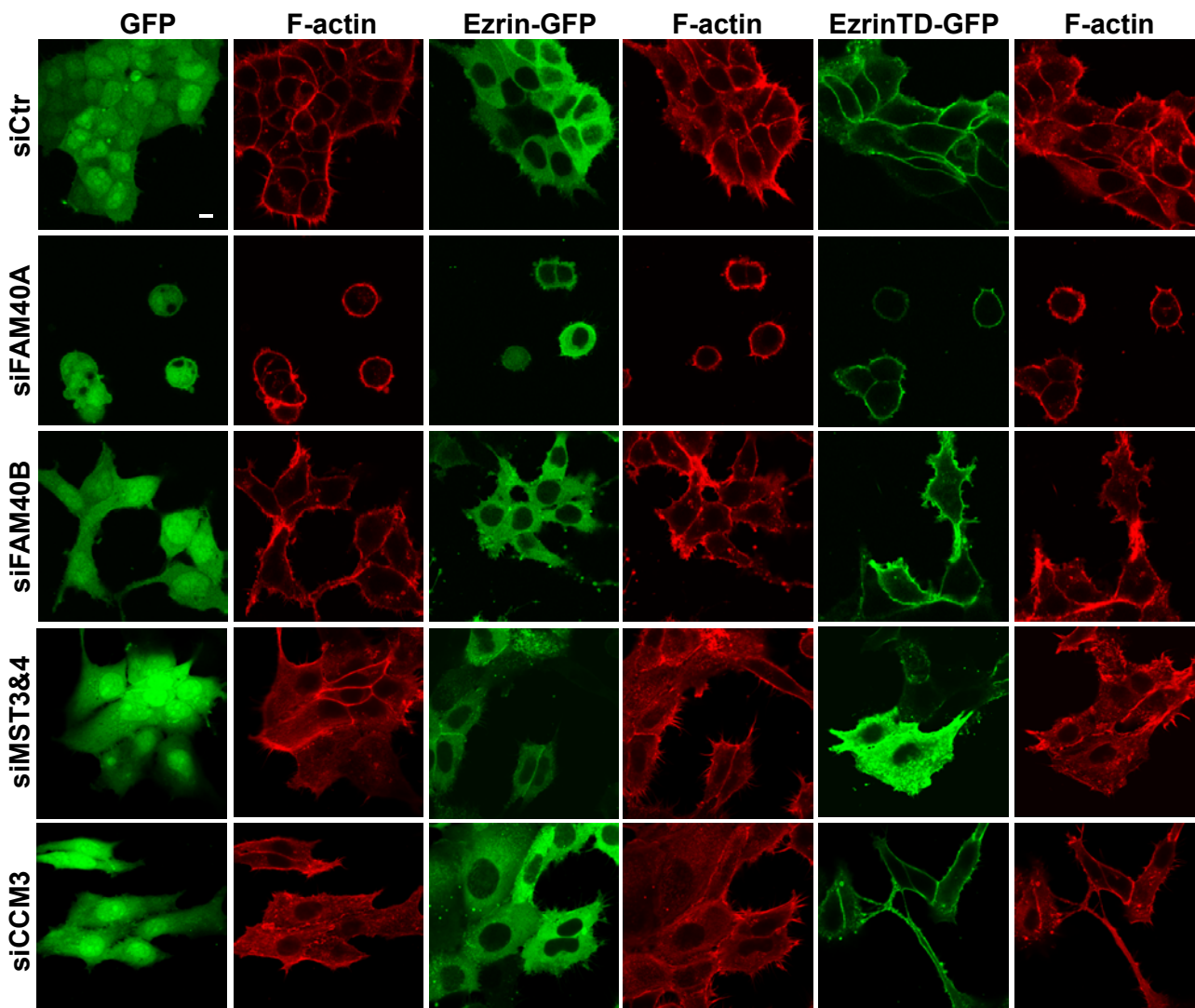
Supplementary Figure 5 Spatial localisation of MLC and Ezrin during migration. (a) Time lapse analysis of the temporal and spatial localisation of MLC-Cherry (red) and Ezrin-GFP (green) in MDA-MB231 cells (left image). White arrow indicates direction of migration. Quantification of the spatial distribution of MLC-Cherry and Ezrin-GFP intensities +/-s.e.m. (n=14 cells). Unpaired student's t-test (two-tailed), *** $P < 0.001$. Left histogram shows MLC-Cherry in the front and rear of the cells. Right histogram shows the Ezrin-GFP in the front and rear of the cells. (b) 2D migration analysis of siRNA transfected MDA-MB231 cells stably expressing either H2b-GFP were generated using MetaMorph Software. Motion analysis and migration tracks were generated from H2b-GFP images taken over 12h at 5 minutes intervals. Analysis of 2D migration persistency using Mathematica

Software. Box and Whiskers graph: Line = Median, Box = distribution of 50% of values, Whiskers = 20-80 percentile. n=fields of cells (10x); (siCtr, 34; siFAM40A, 37; siFAM40B, 30; siMST3&4, 35; siCCM3, 32). (c) Schematics of the computational model to investigate the effect of perturbing the co-localisation of actomyosin contraction and actin cortex to plasma membrane attachment during migration through channels that are 8 μ m wide and 6.5 μ m long. These dimensions correspond to those of commercially available transwell chambers. The model predicts that co-localisation favours migration through 8 μ m channels. All statistical test were performed using 1way ANOVA, Sidak's multiple comparison test, unless stated otherwise, ** $P < 0.01$, *** $P < 0.001$. All experiments were conducted at least 3 independent times. Scale bar, 10 μ m.

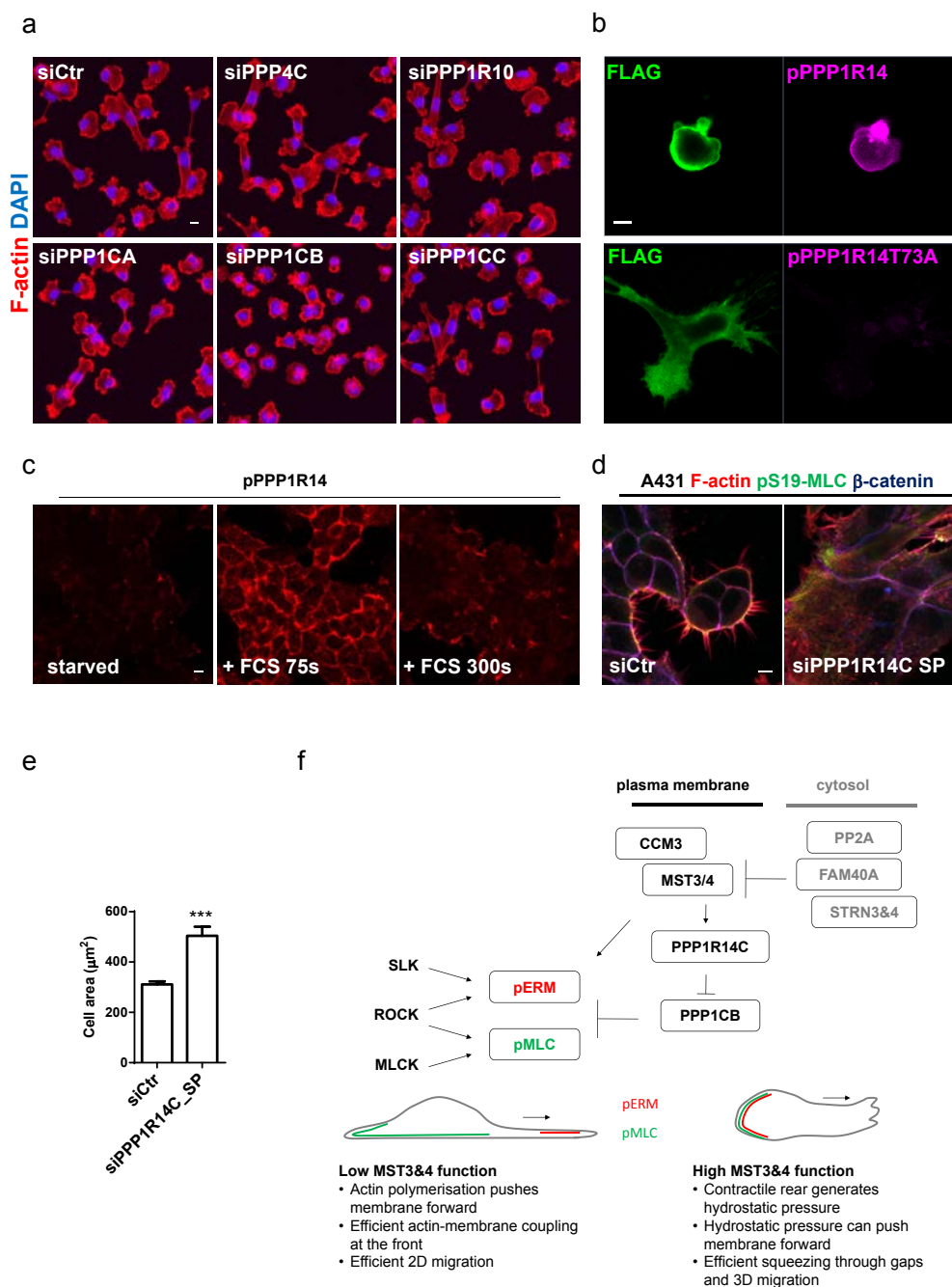


Supplementary Figure 6 Clinical significance of MST3, MST4 and CCM3 expression in breast cancer patients. **(a-b)** Immunoblotting analyses demonstrating the levels of endogenous MST3 and FAM40A (grey arrows) and exogenously expressed MST3-GFP and FAM40A-GFP (black arrows) in A431 **(a)** and MDA-MB231 cells **(b)**. **(c)** Analysis of publicly available datasets show the mRNA log₂ expression levels of MST3, MST4, CCM3, STRN3 and STRN4 observed in human breast cancer patients (n=1881 patients). The statistical analysis was based on human cancer subtypes (left panels), ER-status (middle panels), and disease grade (right

panels). The box plots are made with default parameters to the box plot function in R. Box and Whiskers graph: line=median, box=interquartile range (25%-75%), and the whiskers extend to the most extreme data point which is no more than 1.5 times the interquartile range from the box. **(d)** Immunoblotting analysis of striatins and pMST3&4 upon siRNA depletion in MDA-MB231 cells. **(e)** Tumour Cell Genome Atlas (TCGA) data on cBioportal demonstrating the frequency of mutation, deletion, amplification, and multiple alteration for human FAM40A/STRIP1 and FAM40B/STRIP2.



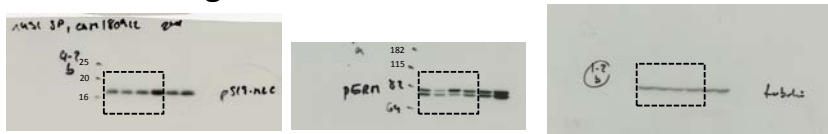
Supplementary Figure 7 Spatial ERM translocation is the outcome but not the course of the morphological changes observed upon FAM40A&B, MST3&4 and CCM3 depletion. Stable ectopic overexpression of wild type Ezrin-GFP or constitutive active Ezrin-T567D-GFP (EzrinTD) in A431 cells did not rescue the cell morphology changes observed upon FAM40A, FAM40B, MST3&4, and CCM3 depletion. All experiments were conducted at least 3 independent times. Scale bar, 10 μ m.



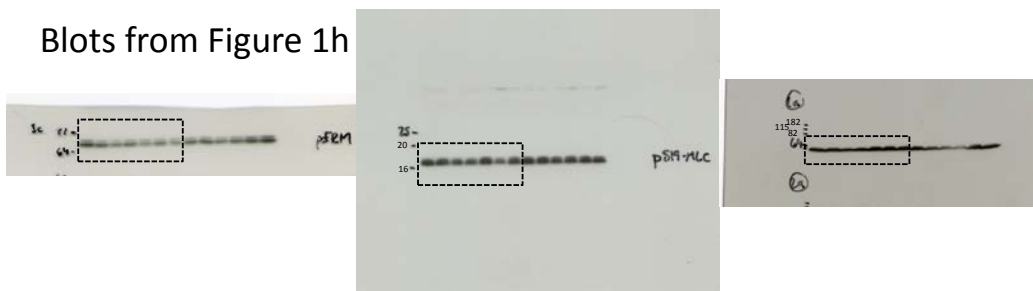
Supplementary Figure 8 PPP1CB and PPP1R14C regulate cell morphology (a) Characterisation of morphological phenotype in MDA-MB231 cells upon siRNA depletion of five phosphatases used in the original screen. F-actin is stained with Phalloidin-TRITC (red) and the nucleus is stained with DAPI. (b) The phospho-specific PPP1R14A antibody is a pan-PPP1R14 antibody as it also binds specifically to overexpressed wild type PPP1R14C but not the T73A point mutant. (c) Serum stimulation of serum starved A431 cells stimulates translocation and phosphorylation of PPP1R14 at cell-cell junction and cell edges with the same kinetics as MST3 translocation. (d) Immunofluorescence analysis of pS19-MLC (green), F-actin (red) and β -catenin (blue) in PPP1R14C depleted A431 cells. (e) Quantification of A431 cell area +/-s.e.m upon depletion of PPP1R14C using siRNA smart pools (n=fields of cells; Ctr, 31; 14C, 27). Statistical test were performed using unpaired student's t-test (two-tailed), * $P < 0.05$, ** $P < 0.01$, *** $P < 0.001$. All experiments were conducted at least 3 independent times. Scale bars, 10 μ m. (f) Working model. The

STRIPAK complex controls the spatial regulation of actomyosin and ERM activities at cell-cell junction and cell edges. The STRIPAK complex thereby acts in synergy with other regulators of contractions, such as RhoA/ROCK. The STRIPAK complex is composed of PP2A phosphatases that can inactivate the kinases MST3&4 within the complex. PP2A is directed to the activation loop of the kinases by the scaffolding proteins FAM40A and FAM40B1, while FAM40B2 cannot bind PP2A catalytic sub-units and acts as a competitive inhibitor. CCM3 recruits MST3&4 to sites of actomyosin contraction where it phosphorylates and activates members the PP1 phosphatase inhibitor family, PPP1R14A-D, leading to increased contraction. MST3&4 may also directly phosphorylate ERM proteins. Ultimately, the STRIPAK complex determines if the actomyosin network is coupled to the plasma membrane (ERM). Low MST3&4 activities couple the actomyosin network to the ECM and favour 2D migration, while high MST3&4 activities couple the actomyosin network to the plasma membrane facilitating 3D migration through confined environment.

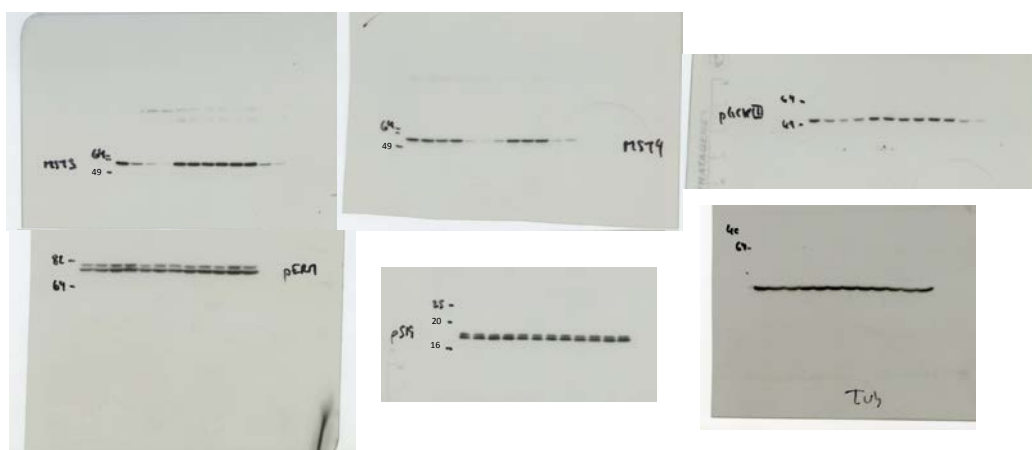
Blots from Figure 1d



Blots from Figure 1h



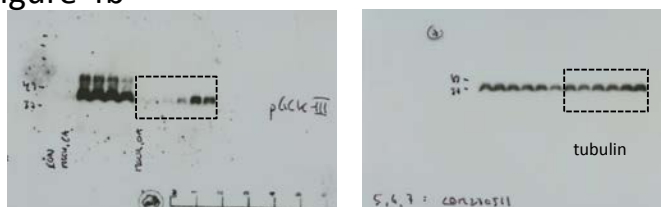
Blots from Figure 3b



Blots from Figure 4a

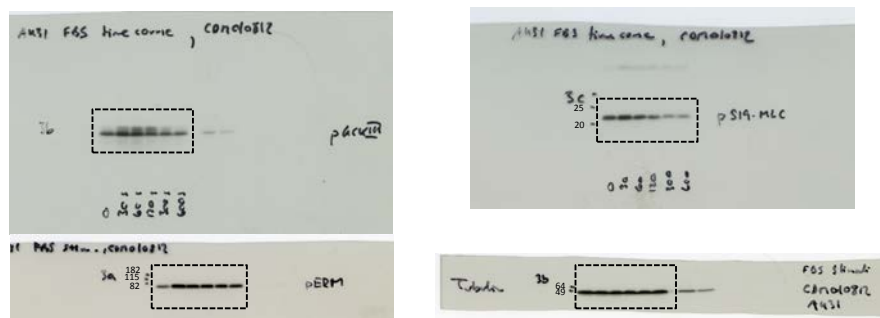


Blots from Figure 4b

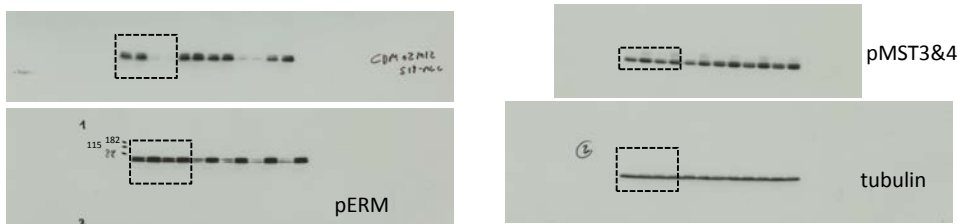


Supplementary Figure 9 Original uncropped western blots.

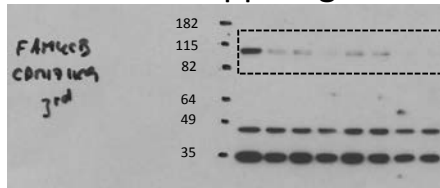
Blots from Figure 5d



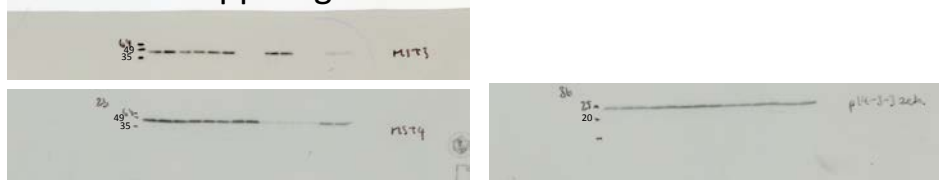
Blots from Figure 5f



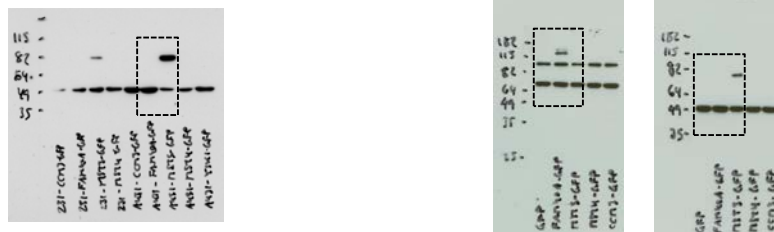
Blots from Suppl. Figure 2c



Blots from Suppl. Figure 3c

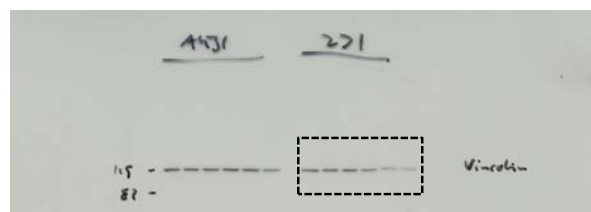


Blots from Suppl. Figure 6a&b



Supplementary Figure 9 continued Original uncropped western blots.

Blots from Suppl. Figure 6d



Supplementary Figure 9 continued Original uncropped western blots.

Supplementary Table Legends

Supplementary Table 1 Information of the siRNA screen's. Sheet 1. Fly screen. List of genes that were depleted in the fly screen. Sheet 2. Fly genes and human homologous. Genes with similarities are also included. Sheet 3. siRNA sequences and catalogue number of all siRNA used in the screen. All siRNA's were purchased by Dharmacon. Sheet 4. Fly and human gene names, fly and A431 phenotypes.

Supplementary Table 2 Peptide kinase screen. Peptide sequences and specific phospho site are shown. Raw data from each experiment is shown.

Supplementary Table 3 qPCR primers and siRNA oligo's. qPCR primer sequences and siRNAs used in the study including catalog numbers.

Supplementary Table 4 Expression vectors. All expression vectors used in this study are shown.

Supplementary Table 5 Antibodies. All antibodies used in this study including provider, catalog numbers and dilutions are shown.

Supplementary Video Legends

Supplementary Video 1 3D morphologies of siRNA depleted A431 cells. 3D reconstruction of confocal stacks taken of siRNA transfected A431 cells stained for F-actin (red) and pS19-MLC (green). The cells were plated on top of collagen-1/matrigels. The movie includes siCtr, siFAM40A, siFAM40B and STRN3 depleted A431 cells sequentially.

Supplementary Video 2 Spatiotemporal regulation of MST3-GFP. Confocal time lapse movie of siRNA transfected A431-MST3-GFP cells. The cells have been serum starved for 24h and then stimulated with FBS. Imaging is then initiated immediately and frames are taken every 20 seconds. When cells were treated with ROCK inhibitor (Y27632) the drug was added during serum starvation. The movie includes siCtr, ROCK inhibitor (Y27632) treated, and siCCM3 depleted A431-MST3-GFP cells sequentially.

Supplementary Video 3 Time-lapse movie of siRNA depleted MDA-MD231 cells on hard surfaces. Phase contrast time lapse movie of siRNA transfected MDA-MB231 cells plated on a 2D planar surface. Images were taken every 5 min. The movie includes siCtr, siFAM40A, siFAM40B and siMST3&4 depleted MDA-MB231 cells sequentially.

Supplementary Video 4 Time-lapse movie of siRNA depleted MDA-MD231 cells on soft surfaces. Phase contrast time lapse movie of siRNA transfected MDA-MB231 cells plated on top of collagen-1/matrigels. Images were taken every 5 min. The movie includes siCtr, siFAM40A, siFAM40B and siMST3&4 depleted MDA-MB231 cells sequentially.